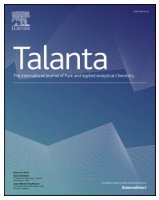
Talanta 266 (2024) 125081



Contents lists available at ScienceDirect

Talanta

journal homepage: www.elsevier.com/locate/talanta





Monolithic 3D structural-substrate SERS sensing platform for ultrasensitive and highly-specific analysis of trace bisphenol A

Zhixin Li [a,1], Qian Xie [b,1], Jinxin Chi [b], Hui Chen [d], Zhuling Chen [a], Xucong Lin [a,c,*], Guihua Huang [b,**]

[a] Institute of Food Safety and Environment Monitoring, Fuzhou University, Fuzhou, 350108, PR China
[b] Xiamen Key Laboratory of Food and Drug Safety, College of Environment and Public Health, Xiamen Huaxia University, Xiamen, 361024, PR China
[c] Engineering Technology Research Center on Reagent and Instrument for Rapid Detection of Product Quality and Food Safety in Fujian Province, Fuzhou University, Fuzhou, 350108, PR China
[d] State Key Laboratory of Photocatalysis on Energy and Environment, College of Chemistry, Fuzhou University, Fuzhou, 350108, PR China

ARTICLE INFO

Handling editor: Ian D McKelvie

Keywords:
Aptasensor
Bisphenol A
Monolith
Surface-enhanced Raman spectroscopy
3D structural-substrate

ABSTRACT

Constructing advanced substrates with excellent features is promising for sensitive surface-enhanced Raman spectroscopy (SERS) detection. Here a novel capillary monolithic 3D structural-substrate SERS platform with Au@cDNA@Ag@Cyanine 3-aptamer nanoparticles (Au@cDNA@Ag@Cy3-Apt NPs) was fabricated for rapid, highly specific profiling of ultra-trace Bisphenol A (BPA). The proposed SERS platform combined both in-capillary SERS and aptamer-affinity recognition strategies, in which the superior SERS properties of Au–Ag NPs, aptamer selectivity, and the advantages of capillary monolith were integrated. A 3D hierarchically porous network was constructed in the monolithic column, which was endowed with rich hotspots for SERS, rapid sample permeation, and better analysis efficiency than most plane-shaped SERS modes. By varying the amount of Ag^{+} precursor, the Ag-shell thickness on SERS was finely tuned to guarantee Cy3 label in proximity to the plasmonic surface. Based on the biorecognition of aptamer, the selective identification of BPA occurred and exhibited a significant change in SERS intensity without obvious interference. As a result, the monolithic SERS platform featured facile operation, excellent specificity, and rapid analysis (10 min, much less than the solution-based or planar substrate SERS modes). Ultra-high sensitivity and robust reproducibility for BPA analysis was achieved with a low limit of detection (LOD) at 9.12×10^{-4} ng/L. The feasibility of this SERS platform for monitoring BPA in water and milk samples was also validated. This work lights a new access to capillary monolithic SERS-sensing platform for ultrasensitive and specific analysis of BPA.

1. Introduction

Rapid, sensitive, and specific sensing monitoring of environmental contaminants for guaranteeing human health has received much attention [1–3]. Bisphenol A (BPA), a plasticizer used intensively in plastics manufacturing, is considered as a selective estrogen receptor modulator (SERM) and has been shown to play a role in the pathogenesis of several endocrine disorders [4,5]. BPA is included in the endocrine-disrupting chemical (EDC) group and may cause negative effects on human health even at a low concentration [6,7]. The European Union (EU) stipulates that the maximum residue limit (MRL) of BPA in the production of food packaging materials is 0.05 mg/kg [8,9]. Effective monitoring of BPA is necessary and has aroused wide concern. However, BPA is generally found in low levels in the environment, and coexisting substances are often present in high concentrations, which might cause a detection deviation if the analytical method lacks enough sensitivity and specificity. So, developing a sensitive, highly-selective protocol for highly-specific and precise analysis of trace BPA is well-welcomed.

Currently, traditional chromatography methods such as high-performance liquid chromatography (HPLC) [10] coupled with a fluorescence detector (HPLC-FLD) or a diode array detector (HPLC-DAD) [13,14], have been developed for the determination of BPA. HPLC-mass

* Corresponding author. Institute of Food Safety and Environment Monitoring, Fuzhou University, Fuzhou, 350108, PR China.
** Corresponding author.
E-mail addresses: xulin@fzu.edu.cn (X. Lin), huanggh@hxxy.edu.cn (G. Huang).
[1] These authors contributed equally to this work.

https://doi.org/10.1016/j.talanta.2023.125081
Received 11 March 2023; Received in revised form 10 August 2023; Accepted 14 August 2023
Available online 15 August 2023
0039-9140/© 2023 Elsevier B.V. All rights reserved.

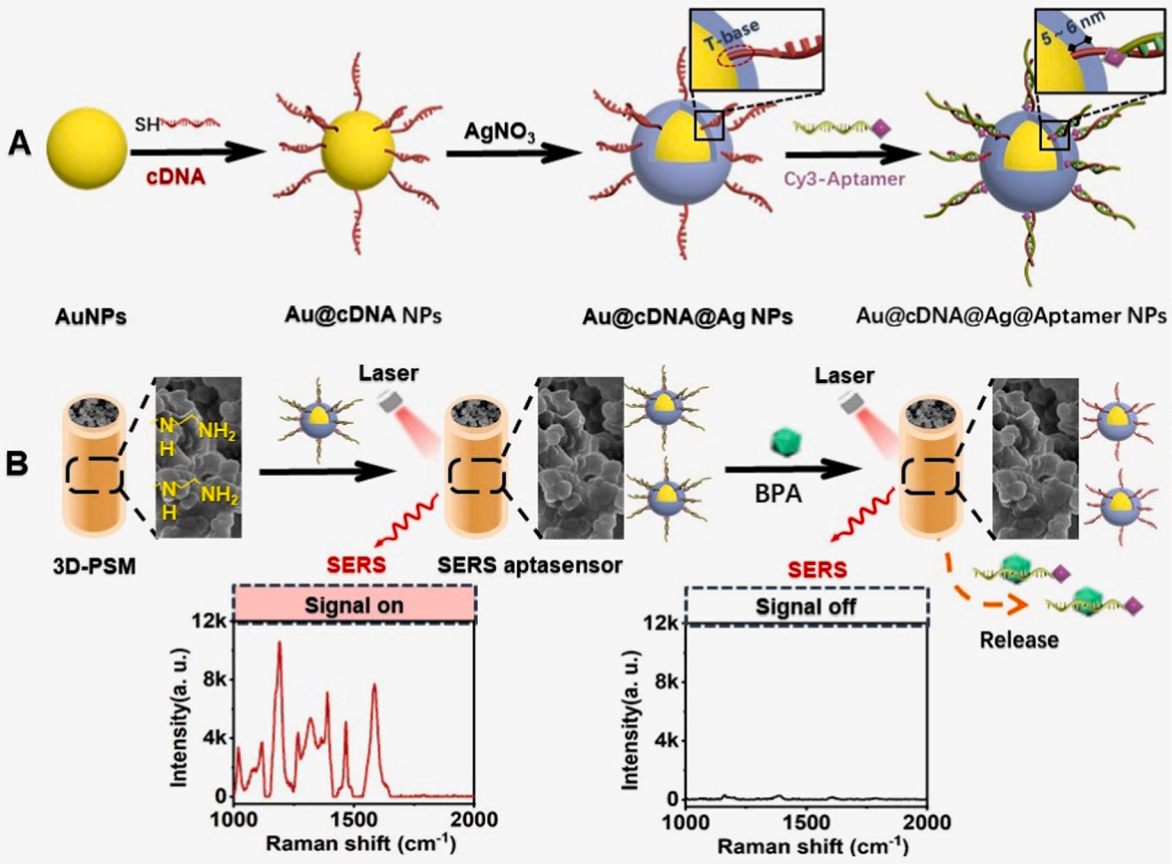


Fig. 1. Schematic demonstration of the fabrication of a SERS aptasensor using a 3D porous silica monolith (3D-PSM) for rapid and specific detection of BPA.

spectrometry (HPLC-MS) [11] or gas chromatography-mass spectrometry (GC-MS) [12] is recommended as the standard method to detect BPA by the regulation in force. High resolution and good reproducibility exhibit in these technologies, while expensive instruments, high costs, tedious sample pretreatment procedures, and skilled operations are required. Immunoassay analysis is also adopted for identifying the BPA molecule, while it might suffer from the tedious preparation of animal antibodies and limited tolerance in a complex environment. Interestingly, surface-enhanced Raman spectroscopy (SERS) sensors have emerged as a robust strategy for monitoring trace BPA [15,16]. Via fabricating a SERS substrate capable of capturing target molecules in proximity to the surface of noble metals (e.g., Au, Ag, etc.), the construction of plasmonic nanostructures containing high-density "hot spots" was adopted to improve signal enhancement. SERS sensing platform for monitoring BPA molecules with a dramatic enhancement of Raman intensity has been intensively reported [17–19]. Based on the solution or planar substrates, SERS sensors such as graphene oxide (GO)-Au nanospheres (AuNSs)-based, AuNPs-Au nanorods (AuNRs)--based, single-atom catalyst (SAC) amplification AuNPs-based, or Au/Ag core-shell nanoprobes-based SERS platforms, have been put forward with sensitive, specific and non-destructive features [20–22]. Nevertheless, the recognition of traditional substrate-based SERS platforms suffered from a long-time detection period from 40 min to 2 h, even 12 h, which was time-consuming and inhibited the detection efficiency for rapid monitoring.

As an alternative, the three-dimensional (3D) SERS substrates with a periodic regular porous structure have attracted considerable interest due to their large effective surface area for introducing metal nanoparticles (NPs) into the porous structures uniformly [23–25]. The 3D porous structures such as metal-organic frameworks (MOFs) [26,27], porous silica [28,29], and gels [30] have been designed to form high-density 3D "hot spots" in the focus volume for effectively trapping target analytes. More "hot spots" were generated and greatly enhanced the SERS signal intensity compared with the traditional planar substrates [31], making them ideal substrates for microanalysis. Several application scenarios of 3D SERS substrate-based platforms have been made for trace analysis such as Rhodamine 6G [25], 4′-mercapto-biphenylcarbonitrile (BPTCN) [26], and phosmet residues [28]. However, for those molecules such as BPA without active sites such as sulfhydryl or amino groups, the sensitive SERS profiling is still up against some difficulty because these analytes could not effectively contact with the surface of noble metal to excite the SERS signal enhancement [32,33]. Furthermore, selective adsorption was still absent in the above traditional SERS methods that were susceptible to contamination in the complicated environment, as hindered a further application of the sensitive trace analysis. Challenges remain in developing a good strategy to selectively identify target BPA for rapid, ultrasensitive SERS detection, as well as robust stability, instead of indiscriminately trapping molecules onto the plasmonic surface in the 3D structures.

Herein, a novel capillary monolithic SERS sensing platform with a 3D hierarchically porous network modified by aptamer-conjugated Au@cDNA@Ag NPs was proposed. As shown in Fig. 1, the proposed monolithic SERS platform was fabricated for the first time by decorating cyanine 3-aptamer (Cy3-Apt) conjugated Au@cDNA@Ag NPs on the capillary 3D porous framework. The monolith possessing a hierarchical porous structure was offered to provide a high specific surface area [28,29] and endowed rapid permeation of the mobile phase with a high capture efficiency of target molecules. Cyanine 3 (Cy3-Apt) possesses superiority such as narrow absorption bands, high extinction coefficients, and excellent resistance to photobleaching [34]. By adjusting the amount of $AgNO_3$, the thicknesses of the Ag shell on Au–Ag NPs labeled with Cy3-Apt were finely regulated and the intensity and

reproducibility of SERS signals were guaranteed. In this way, the advantages such as the superior SERS properties of Au–Ag NPs, signal amplification and high capture efficiency in capillary 3D-substrate SERS, and selective biorecognition of aptamer, were integrated synergistically. The morphology of the monolith and the effects of affinity recognition conditions on the SERS performance were featured. Easy operation and micro-sample analysis proceeded, based on the monolithic SERS platform used as the liquid flow channel and detection chamber simultaneously. Au@cDNA@Ag@Cy3-Apt NPs exhibited a highly specific affinity toward BPA and achieved rapid recognition (only 10 min) with a remarkable change of SERS signal. Compared with the previous plasmonic nanostructures used by dispersing aqueous solution [35,36] or planar platform [37,38], a much faster detection time was achieved. Good reproducibility and ultrahigh sensitivity were obtained with high specificity. The as-designed monolith-based SERS platform demonstrated an attractive access for superior capabilities toward the rapid specific microanalysis of trace BPA with high selectivity, controlled hot-spot assembly, and significant SERS enhancement in a 3D monolithic structure.

2. Materials and methods

2.1. Chemicals and materials

N-(2-aminoethyl)-3-aminopropyltriethoxysilane (AEAPTES), tetraethyl orthosilicate (TEOS),cetyltrimethylammonium bromide (CTAB), citrate acid (CA), L-ascorbic acid (AA), gold (III) chloride trihydrate ($HAuCl_4{\cdot}3H_2O$), silver nitrate ($AgNO_3$), 6-mercapto1-hexanol (MCH), and tris(hydroxymethyl)aminomethane hydrochloride (Tris-HCl) were purchased from Aladdin Industrial Co. (Shanghai, China). Bisphenol A (BPA) (certified reference material), 4,4-dihydrxytetraphenylmethane (BP), bisphenol B (BPB), bisphenol C (BPC), and tris(2-carboxylethyl) phosphine hydrochloride (TCEP) were purchased from Sigma-Aldrich (USA).

According to ref. [35], Cy3-labeled aptamer for BPA (5′-Cy3-CCG GTG GGT GGT CAG GTG GGA TAG CGT TCC GCG TAT GGC CCA GCG CAT CAC GGG TTC GCA CCA) and Sulfhydryl labeled cDNA (3′–SH–C3-TTT TTT TTT TGG CCA CCC ACC AGT CCA C) were fabricated by Sangon Biotech. Co. (Shanghai, China). The initial milk and mineral water samples were purchased from the local supermarket. The blank mineral water is marked with MW-0, and the mineral water samples prepared under simulated heating statuses of 40 °C, 50 °C, 60 °C and 70 °C for 1 h are marked with MW-1 to MW-4, as well as MW-5 to MW-9 foe heating 3 h and MW-10 to MW-14 for heating 5 h, respectively. Similarly, the blank milk sample is marked with Milk-0, and the milk samples prepared under simulated heating statuses of 50 °C, 60 °C, 70 °C, 80 °C, 90 °C and 95 °C for 5min are marked with Milk-1 to Milk-6, respectively. The binding buffer solution (BB) (Tris-HCl 10 mM, $CaCl_2$ 20 mM, NaCl 120 mM, KCl 5.0 mM) with pH 7.40 was used. The quartz capillary (inner diameter of 100 μm) was purchased from the Yongnian optic fiber plant (Hebei, China). Ultrapure water with resistivity up to 18.2 MΩ cm^{-1} at 25 °C was provided by a Milli-Q purification apparatus (Millipore Corporation, USA).

2.2. Synthesis of AuNPs decorated with cDNA

AuNPs (12–60 nm) were synthesized according to the previous reference [28]. A 100 mL of aqueous $HAuCl_4$ solution (wt 0.01%) was heated to the boiling point under vigorous stirring. Then, a series of freshly-prepared citrate acid solution (3.0, 2.0, 1.5 and 0.75 mL) were added, respectively. After boiling for 60 min and the mixture solution then cooled to 25 °C under the vigorous stirring.

As shown in Fig. 1, the cDNA sequences were immobilized on AuNPs via the Au–S bonds, and the Au@cDNA NPs were obtained. cDNAs were consequently dissolved in a Tris-HCl buffer (10 mM Tris-HCl, 120 mM NaCl, 1 mM KCl, pH 7.40). The mixture was heated to 90 °C for 3 min and slowly cooled to 25 °C in a water bath. The obtained solution was mixed with 10 μL of 10 mM TCEP and incubated for 2 h at 25 °C to reduce the disulfide bond. Finally, this obtained solution was diluted with a Tris-HCl buffer to achieve the concentration of cDNAs of 100 μM.

Then 10 mL of the AuNPs dispersions (0.005 wt%) were mixed with 10 μL of the cDNAs solution (1 μM) with the ratio of AuNPs to the cDNAs solution of 1000:1 (v/v). The mixture was oscillated for 2 min at room temperature and then placed it in a thermo-shaker (4 °C, 800 rpm) for 24 h to form covalent Au–S bonding between the terminal thiolate group of cDNA and AuNPs. To consolidate the connection of AuNPs and cDNAs, 60 μL of NaCl solution (1 M) was added into the mixture in three stepwise. 30 μL of 6-mercapto1-hexanol (MCH, 10 μM) was added to occupy the nonspecific binding on AuNPs. After being stored at 4 °C for 24 h, the solution was centrifuged at 6080 g for 30 min to remove unbound chemicals and cDNAs. Finally, the Au@cDNA NPs were redispersed in the ultrapure water.

2.3. Synthesis of Au@cDNA@Ag@Cy3-Apt NPs

Firstly, Au@cDNA@Ag NPs were prepared as below. 3 mL of Au@cDNA NPs solution and 13.4 mL of ultrapure water were mixed in a 50 mL round bottom flask and kept stirring at room temperature (800 rpm) for 5 min. Then, 60 μL of 1.0% L-ascorbic acid solution and 60 μL of 1.0% citrate acid solution were added into the above diluted Au@cDNA NPs solution and kept stirring for 15 min 60 μL 10 mM $AgNO_3$ solution was slowly dropped stepwise into the above mixture solution at a rate of 10 μL/min under vigorous stirring. The color of the mixture changed from wine red to orange. Finally, the Au@cDNA@Ag NPs solution was centrifuged to remove unreacted reagents and redispersed in ultrapure water.

As shown in Fig. 1, aptamers were immobilized on Au@cDNA@Ag NPs via hybridization reaction between complementary base pairing of cDNA and aptamer, and the Au@cDNA@Ag@Cy3-Apt NPs were consequently obtained. Firstly, the BPA aptamers were dissolved in the Tris-HCl buffer. 2 μL of 100 μM aptamers solution was added into the above diluted Au@cDNA@Ag NPs solution. The obtained solution was heated to 95 °C for 5 min and then slowly cooled down to room temperature. After a centrifugation procedure, the Au@cDNA@Ag@Cy3-Apt NPs were redispersed in ultrapure water, and stored at 4 °C for further application.

2.4. Fabrication of 3D SERS aptasensor

As shown in Fig. S1, the porous silica monolith with a porous structure was used to prepare the 3D SERS aptasensor. Based on the optimal recipe (Table S1, in ESI), the synthesis of silica monolith was fabricated according to ref. [28]. The polymerization solution was a homogeneous mixture consisting of CTAB, water and ethanol (porogen reagent), as well as AEAPTES and TEOS monomers. Briefly, 11.1 mg of CTAB, 200.0 μL of ethanol, and 50.0 μL of water were mixed and ultrasonicated at 0 °C for 30 s. Then, 40.0 μL of AEAPTES and 160.0 μL of TEOS were added to the above mixture solution and followed by ultrasonication at 0 °C for 5 min to form a homogeneous solution. The obtained solution was pumped into the pretreated capillary. The capillary was then immersed in a thermostatic water bath at 40 °C for 24 h with both ends sealed with silicon rubbers. The silicon rubbers were removed and the capillary filled with wet gel was heated at 120 °C for 3 h. Finally, the residual reagents were flushed out from the capillary by rinsing with ethanol and water.

To build the 3D SERS aptasensor, the prepared porous silica-based monolith was initially cut into pieces of 1 cm length. 200 μL of Au@cDNA@Ag@Cy3-Apt NPs solution was pumped through the 1 cm length monolithic column at a rate of 20 μL/min. To remove residual Au@cDNA@Ag@Cy3-Apt NPs, the monolithic column was rinsed with ultrapure water. Finally, the obtained 3D SERS aptasensor was filled with Tris-HCl buffer solution and stored at 4 °C before use.

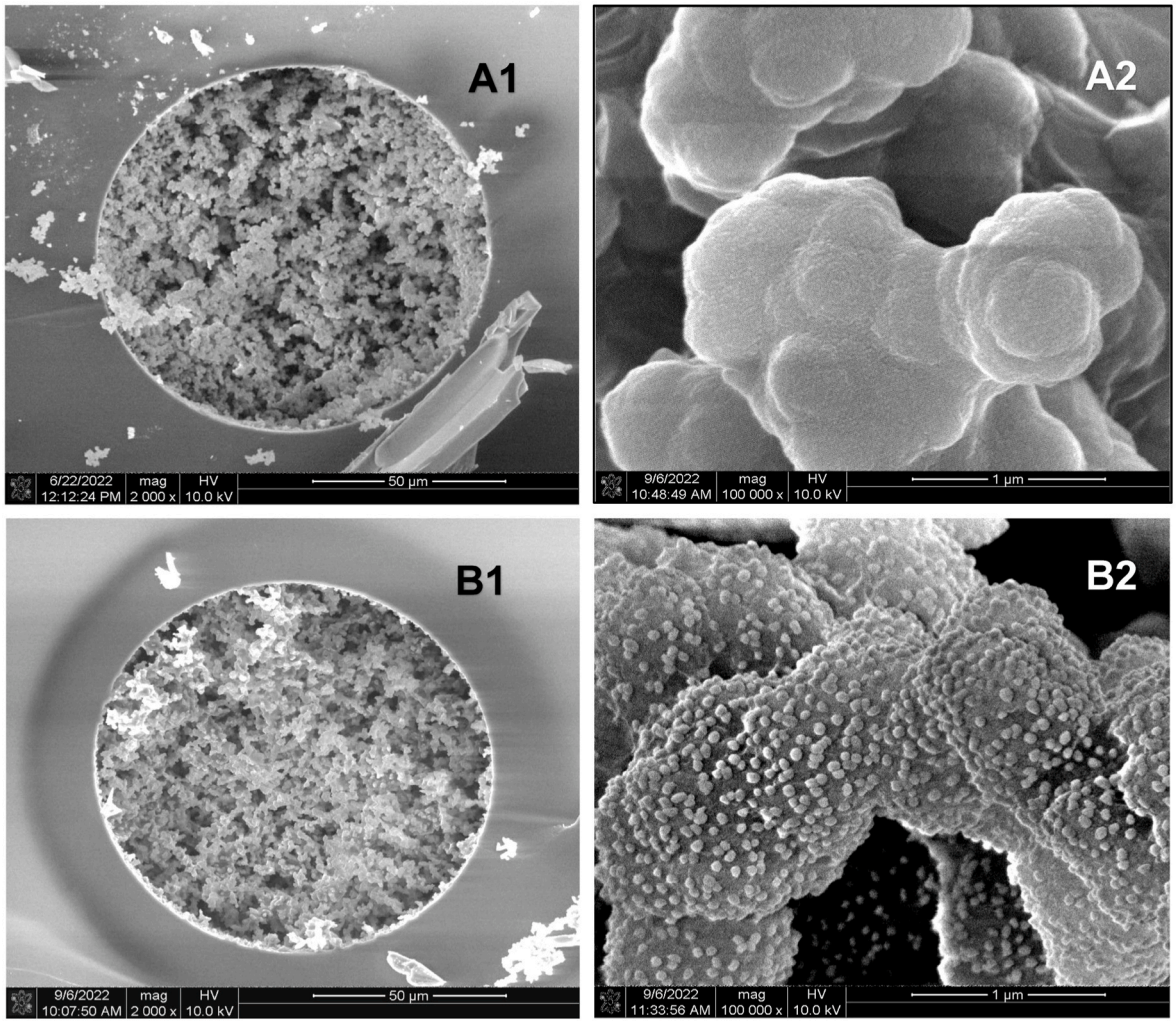


Fig. 2. Representative SEM images of the porous silica monolith (3D-PSM) (A1: × 2,000, A2: × 100,000) and the 3D-PSM modified with Au@cDNA@Ag@Cy3-Apt NPs (B1: × 2,000, B2: × 100,000).

2.5. Characterization

The transition electron microscope (TEM) images of Au and Au@cDNA@Ag@Cy3-Apt NPs were examined by a transmission electron microscope (Tecnai G2 F20, FEI, America) operating at an accelerating voltage of 200 kV, and the TEM mapping were measured by a high-resolution transmission electron microscope (FEI Talos F200x, America) operating at an accelerating voltage of 200 kV. The size distribution of AuNPs and Au@cDNA@Ag NPs were measured by dynamic light scattering (DLS, BeNano 90 Zeta, Dandong Baxter, China). The UV-visible spectra of metal nanoparticles were recorded with a UV-visible spectrophotometer (UV-2600i, Shimadzu, Japan). EDS elemental analysis, microstructures and morphology measure of the porous silica monolith were examined by scanning electron microscopy (Nova Nano SEM 230, FEI, America).

2.6. Detection of BPA and specificity evaluation

For BPA detection, 30 μL of BPA solution with concentrations from 1.0×10^{-14} to 1.0×10^{-8} M were pumped through the monolithic SERS aptasensor at the flow rate of 3.0 μL/min. The SERS spectra were analyzed by a microscopic Raman spectrometer (ATR 8300 AF, Optosky, China) with a 785 nm laser. A 20 × objective lens was set to focus on the center of the capillary, perpendicular to the axial direction (a depth of 200 μm below the outer surface of the capillary) and the laser power was 120 mW. The integration time was 6000 ms for each scan. At least six spectra from different spots were collected within a Raman shift window between 200 and 2000 cm^{-1}. The mean signal intensity of Raman spectra was adopted for the analysis.

Besides, the mixture composed with BPA and its analogues (viz. BP, BPB, and BPC) were detected by using this SERS aptasensor, and the specificity of this 3D SERS aptasensor for BPA was evaluated.

2.7. Preparation of samples

The samples were prepared according to ref. [39]. Mineral water and Minjiang river water (Fuzhou) were filtered through a 0.22 μm polyethersulfone (PES) filter membrane before testing. Milk products were purchased from a local supermarket. 2 mL of milk solution was centrifuged at 13680 g and 4 °C for 30 min. Then, the yellowish liquid was taken from the middle layer and filtered through a 0.22 μm PES filter membrane before testing. For SERS analysis, the procedures were done as descripted in Section 2.6.

3. Results and discussion

3.1. Principle of monolithic SERS sensing platform

The principle of the proposed monolithic SERS aptasensor for BPA analysis was illustrated in Fig. 1. The SERS aptasensor came into play via

a 3D porous silica-based monolith (3D-PSM) modified with Au@cDNA@Ag@Cy3-Apt NPs. The rich-pore structure and large specific surface area of the 3D-PSM endowed a high density of Au@cDNA@Ag@Cy3-Apt NPs, which allowed BPA efficiently contact with aptamers in the capillary. By regulating the amount of $AgNO_3$, the Ag shell deposition were finely regulated and the Au@cDNA NPs were encapsulated. SERS tag Cy3 was labeled in proximity to the surface of Au–Ag NPs and assembled uniformly on the surface of 3D-PSM (Fig. 1-A), which produced high-density "hot spots" and exhibited a remarkable SERS enhancement for sensing detection.

In this strategy, aptamers in the monoliths were adopted as the specific recognition elements. The BPA-aptamer interactions mainly rely on the structural compatibility and the combination of binding forces, such as hydrogen bonding and hydrophobic effect. If the BPA residue existed, the high-affinity recognition between BPA and aptamer occurred (as shown in Fig. 1-B) [40,41]. BPA was trapped in the hydrophobic active pocket of aptamer surrounded by the side chains of the nucleotides to form stable hydrophobic bonds [42]. In the stem-loop structures of aptamers, hydrogen bonds formed between BPA and the nucleotides. These binding forces promoted the interaction and the formation of the stable binding complex of BPA-aptamer. Based on this strategy, a high-performance recognition of target BPA and Cy3-aptamer happened and aroused the releasing of Cy3-aptamer from the proximity of Au–Ag bimetallic plasma of Au@cDNA@Ag NPs, resulting in a drastic decrease of the SERS signal. The significant decrease of the SERS signal of the system was correlated with the logarithm of BPA content to realize the quantification of BPA.

3.2. Characterization of Au@cDNA@Ag@Cy3-Apt NPs

Based on the strong SERS enhancement of Ag nanoparticles (NPs), Au@cDNA@Ag NPs were formed by depositing Ag on the surface of AuNPs and the superiorities of both AuNPs and AgNPs was integrated. The Au–Ag core-shell NPs were decorated on the 3D monolith for a drastic SERS enhancement. In Fig. S2, TEM images of AuNPs and Au@cDNA@Ag NPs were illustrated, respectively. The relatively uniform size and spherical shape of the selected AuNPs with an average diameter of about 50 nm were observed (Fig. S2-A1, A2). By varying the volume of the $AgNO_3$ solution, the thickness of Ag shell deposited on AuNPs were regulated. In Fig. S2-B1∼B2, the formed Ag shell was closely and homogeneously covered on the Au@cDNA NPs to build Au@cDNA@Ag NPs. The average sizes of Au@cDNA@Ag NPs were measured as ∼60 nm. The thickness of the Ag shell was finely tuned to be 5–6 nm so that it just covered the T-base sequence spacer (shown in Fig. 1 A). The result was consistent with the hydrodynamic sizes of AuNPs and Au@cDNA@Ag NPs measured by DLS (in Fig. S2-A3, B3). The size 5–6 nm of Ag shell maintained a certain gap between the SERS tag Cy3 and the surface of Ag shell [36] and guaranteed a high initial SERS signal for the further BPA analysis.

To identify the structures of Au@cDNA@Ag NPs, the distribution of elements in Au@cDNA@Ag@Cy3-Apt NPs was analyzed by TEM mapping. In Figs. S2–C, the distribution of Au, Ag, and P elements was clearly observed in Au@cDNA@Ag@Cy3-Apt NPs. The Zeta potential of the prepared NPs was also measured. In Fig. S3, the Zeta potential of AuNPs was −29.27 mV, which was mainly due to negatively charged citrate ions on the surface of NPs [36]. The Zeta potential of Au@cDNA NPs, Au@cDNA@Ag NPs and Au@cDNA@Ag@Cy3-Apt NPs were −30.01 mV, −36.18 mV, and −38.26 mV, respectively, which displayed a more negative charge of phosphoric acid groups after hydrolysis compared with AuNPs. It suggested that cDNA and Cy3-aptamer containing phosphate backbone structures were immobilized on Au@cDNA@Ag NPs to form Au@cDNA@Ag@Cy3-Apt NPs.

In Fig. S4, the UV-Vis spectra were also studied to elucidate the changes in surface properties of nanomaterials. The absorption peaks of AuNPs and Au@cDNA NPs were observed at 520 nm and 521 nm, respectively. After depositing the Ag shell and immobilizing Cy3-aptamers on Au@cDNA NPs, a new surface plasmon band appeared at 420 nm for Au@cDNA@Ag@Cy3-Apt NPs. A blue shift of the absorption wavelength of Au from 532 nm to 500 nm was exhibited, indicating the occurrence of silver plasmon resonance on the surface of NPs [41]. The absorption peaks of Au@cDNA NPs, Au@cDNA@Ag NPs, and Au@cDNA@Ag@Cy3-Apt NPs were slightly red-shifted in comparison with that of AuNPs, Au@Ag NPs and Au@cDNA@Ag NPs, respectively. The surface chemistry changes of AuNPs through the replacement of the citrate-ligand layer by cDNA and aptamers, caused the change in the dielectric environment of Au@Ag NPs [36,42].

3.3. Features of monolithic SERS sensing platform

The monolithic SERS aptasensor was constructed by using 3D-PSM as the substrate to be decorated with Au@cDNA@Ag@Cy3-Apt NPs. In Fig. 2, the SEM images of the obtained 3D-PSM substrate and monolithic SERS aptasensor were illustrated, respectively. The 3D-PSM substrate had a uniform porous morphology and rich pore structure (in Fig. 2-A1∼A2), which was favorable to stimulate a significant positive effect on the SERS signal. The rigid silica-based sol-gel skeleton was tightly attached to the capillary inner wall, and formed a hierarchically porous structure with abundant mesopores and macropores. In Fig. 2-B1∼B2, the high-density Au@cDNA@Ag@Cy3-Apt NPs were assembled on the 3D porous framework with good uniformity on the polymer skeleton. Meanwhile, the hierarchically porous morphological structure of the 3D-PSM was still maintained. These porous structures were favorable to obtain active sites and high specific surface area in mesopores and a fast permeation in macropores and rapid response time of aqueous samples.

Element analysis of the 3D-PSM and monolithic SERS aptasensor was carried out by using SEM-EDS. In Fig. S5-A and B, the EDS element distribution of the 3D-PSM (C, O, and Si) and the SERS aptasensor (C, O, Si, Au, and Ag) were clearly displayed, respectively. In Fig. S5 B, the elements of Au, Ag, C, and Si exhibited, which suggested that the Au@cDNA@Ag@Cy3-Apt NPs were successfully modified on the 3D porous networks of the resultant monolith.

Figs. S6–A showed the SERS spectra of the 3D-PSM without modifying Cy3 (Control) and the 3D SERS aptasensor (cDNA was prepared with T-base, noted as with T-base) when the BPA concentration was blank, respectively. No characteristic Raman peaks were observed on the SERS spectrum of the control monolith. For the 3D SERS aptasensor in blank solution (with T-base), the peak of Cy3 at 1188 cm^{-1} (C–H inplane bending), 1393 cm^{-1} (C–N stretching), 1467 cm^{-1} (C=C ring-stretching), and 1590 cm^{-1} (C=N stretching) were recorded respectively (Table S2, in ESI), which was consistent with the previous report [43]. To evaluate the effect of the space between Au/Ag NPs and Cy3 molecules on the SERS enhancement, in Fig. S6-B, the performances of two types of nanoparticles (Au@cDNA NPs were prepared using two types of cDNA with T-base or not, respectively) were evaluated. A stronger SERS enhancement occurred via utilizing Au@cDNA NPs with T-base than that prepared without T-base sequence. In Fig. S6-C, the sensing performance towards BPA was also studied. A strong Raman signal was detected, while a drastic decrease in the SERS signal was achieved with the presence of BPA. The aptamers labeled with Cy3 were released from Au@ cDNA@Ag NPs on the 3D-PSM due to the high affinity between BPA and the aptamer, thus resulting in a drastic SERS decrease. It demonstrated the feasibility of sensitive detection of BPA using the proposed SERS aptasensor.

3.4. Optimization of detection conditions

To obtain the best SERS enhancement, the experimental conditions were optimized. The volumes of $AgNO_3$ and cDNA, and the volume of Au@cDNA@Ag@Cy3-Apt NPs injected into the 3D-PSM were investigated, as well as the injection time of BPA. In Fig. S7, the effect of the size of AuNPs on the SERS response of the aptasensor was tested. The SERS intensity of Cy3 (1188 cm^{-1}) in the monolithic SERS sensing

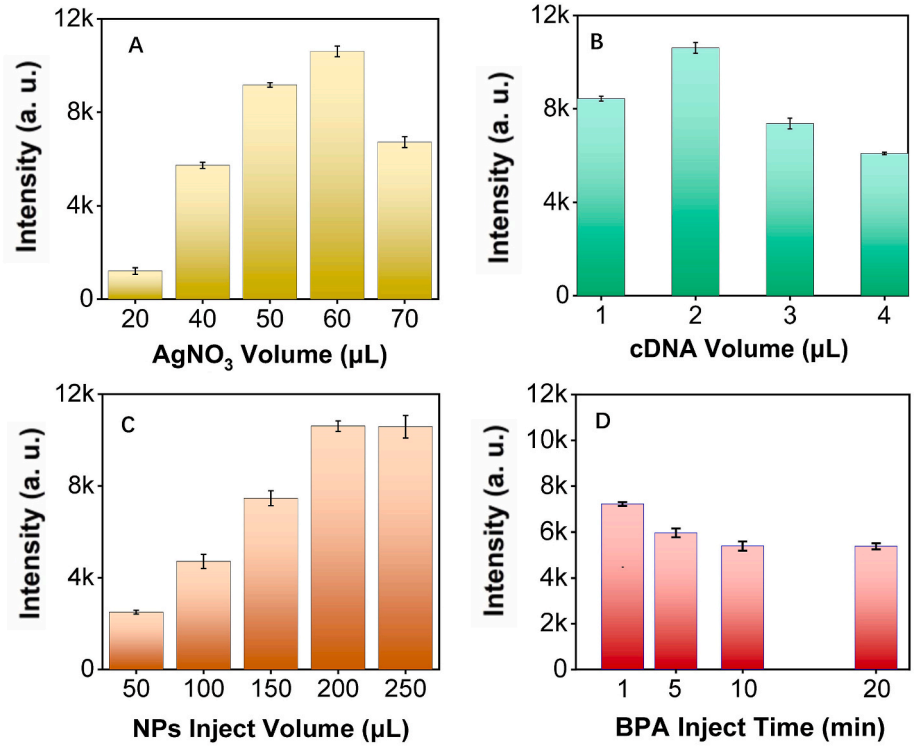


Fig. 3. Effects of different conditions on the SERS intensity at 1188 cm^{-1} of the aptasensors. (A) Volume of $AgNO_3$, (B) volume of cDNA, (C) injection volumes of Au@cDNA@Ag@Cy3-Apt NPs and (D) injection time of BPA, respectively.

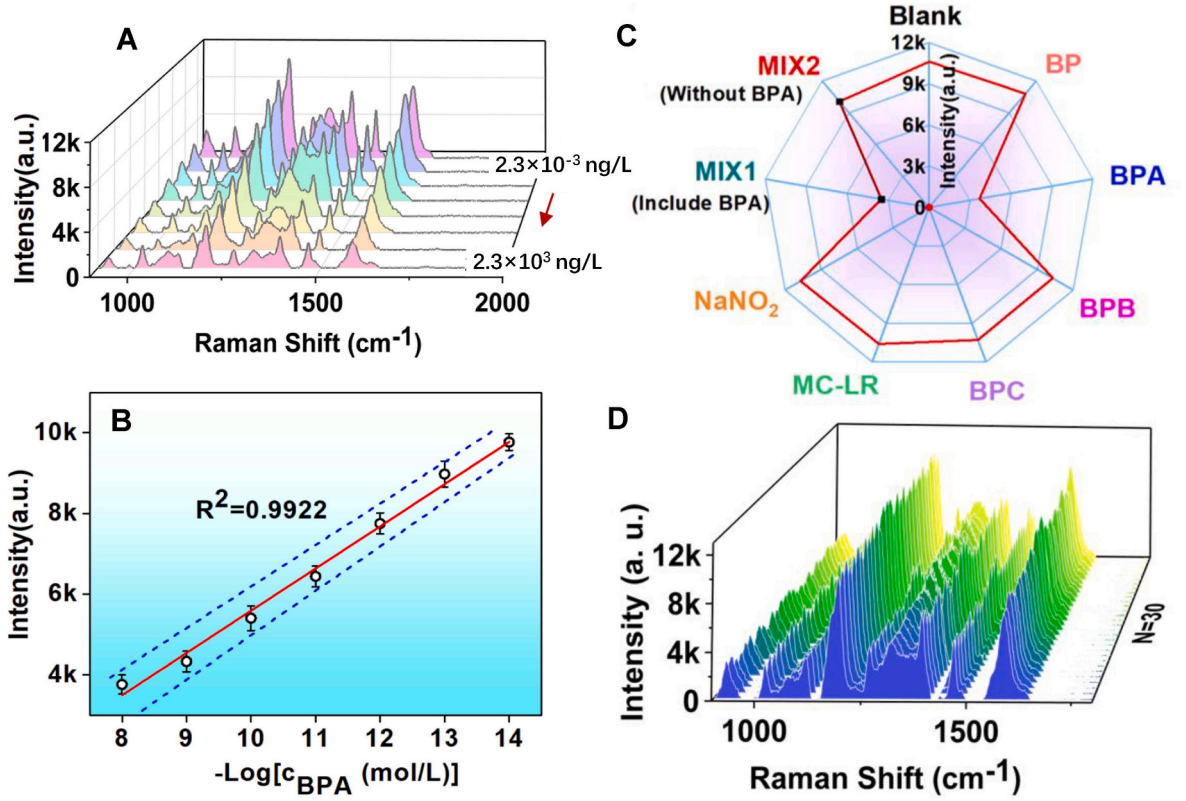


Fig. 4. Evaluation on quantitative analysis, specificity and analysis stability.
A: The Raman spectra of the 3D-SERS aptasensor with different concentrations of BPA. B: The calibration curve of the SERS intensity against BPA at 1188 cm^{-1}. C: the corresponding diagram of SERS peak intensity of various analytes with 1188 cm^{-1} as the center. D: Raman spectra of the 3D-SERS aptasensor acquired from 30 spots at 1188 cm^{-1}.

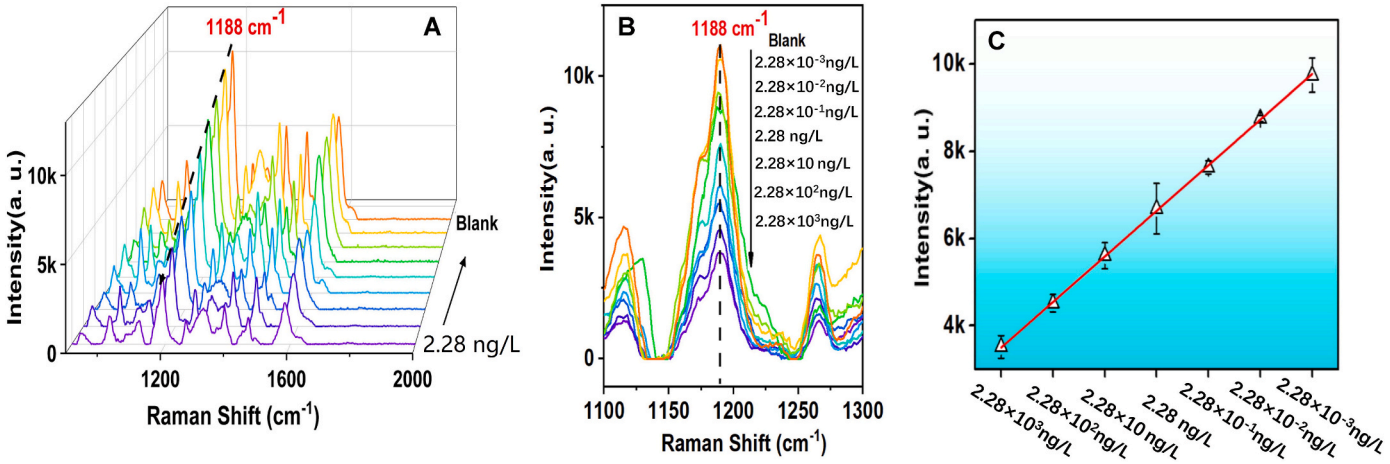


Fig. 5. The SERS spectra of river water spiked with different concentrations of BPA from 2.3 × 10^{-3} to 2.3 × 10^{-3} ng/L (A and B); The calibration curve of SERS intensity of Cy3 at 1188 cm^{-1} against the logarithm of different concentrations of BPA (C).

Table 1
Recoveries of BPA in the fortified river water samples obtained by using the monolithic SERS aptasensor.

Spiked concentrations (ng/L)	Detected concentrations[a] (ng/L)	Recoveries[b] (%)	RSD (%, n = 3)
Original	N.D.	N.D.	N.D. [c]
2.28 × 10^3	(2.23 ± 0.06) × 10^3	94.6 ± 2.9	3.1
2.28 × 10^2	(2.37 ± 0.09) × 10^2	101.3 ± 4.3	4.3
2.28 × 10	(2.44 ± 0.13) × 10	98.3 ± 6.3	6.5
2.28	2.33 ± 0.14	94.1 ± 5.8	6.1
2.28 × 10^{-1}	(2.15 ± 0.17) × 10^{-1}	104.5 ± 7.3	7.0
2.28 × 10^{-2}	(2.46 ± 0.16) × 10^{-2}	102.5 ± 7.0	6.9
2.28 × 10^{-3}	(2.49 ± 0.11) × 10^{-3}	102.8 ± 5.3	5.2

[a] Detected concentrations were presented as mean ± SD, n = 3.
[b] The recoveries were presented as mean ± SD, n = 3.
[c] N.D.: Not detected or under the LOD.

Table 2
Recoveries of BPA in the spiked milk samples obtained by using the monolithic SERS aptasensor.

Spiked concentration (ng/L)	Detected concentrations[a] (ng/L)	Recoveries[b] (%)	RSD (%, n = 3)
Original	N.D. [c]	N.D.	N.D.
2.28 × 10^3	(2.08 ± 0.18) × 10^3	91.0 ± 7.9	8.7
2.28 × 10	(2.50 ± 0.13) × 10	109 ± 5.5	5.1
0.228 × 10^{-1}	(2.22 ± 0.07) × 10^{-1}	97.7 ± 3.0	3.1
2.28 × 10^{-3}	(2.29 ± 0.08) × 10^{-3}	101 ± 3.5	3.5

[a] Detected concentrations were presented as mean ± SD, n = 3.
[b] The recoveries were presented as mean ± SD, n = 3.
[c] N.D.: Not detected or under the LOD.

platform increased rapidly with the size of AuNPs increasing from 12 to 50 nm and got the highest value with the size of AuNPs at 50 nm (Figs. S7–C, in ESI). To gain the optimal thickness of the Ag shell, different contents of $AgNO_3$ were used to form the Ag shell with different thicknesses. As shown in Fig. 3-A and Figs. S8–A, the SERS intensity at 1188 cm^{-1} of the SERS aptasensor increased with the volume of $AgNO_3$ increasing from 30 μL to 60 μL, as the increased thickness of the Ag shell and thus resulting in that Cy3 became closer to the Ag shell. The SERS enhancement decreased if the volume of $AgNO_3$ rose to 70 μL, as the Ag shell was too thick and covered a portion of the bio-recognition sequence of cDNA, resulting in a decreased hybridization rate of chain reaction between cDNA and aptamer. The SERS enhancement at 1188 cm^{-1} got the best with $AgNO_3$ solution of 60 μL with the suitable thickness of Ag shell.

In Fig. 3-B and Figs. S8–B, the SERS intensity at 1188 cm^{-1} of the SERS aptasensor increased when the volume of cDNA increased from 1 μL to 2 μL. However, the SERS intensity decreased with the volume of cDNA rising from 2 μL to 4 μL, due to the spacing effect of nucleotides hindering the reaction [36]. When the content of cDNA was too high, resistance from space effect would generate on the surface of NPs and cDNA would entangle with each other due to their short distance, leading to a decreased rate of hybridization chain reaction between cDNA and aptamer. The SERS intensity was the highest at the cDNA volume of 2 μL.

Fig. 3-C and Figs. S8–C demonstrated the relation between the SERS intensity and the Au@cDNA@Ag@Cy3-Apt NPs volume injected into the 3D-PSM. The SERS intensity increased when the volume increased from 50 μL to 200 μL, as the hot spots gradually formed in the 3D-PSM and the SERS signal was enhanced. However, the SERS intensity stabilized after 200 μL because of the saturation of Cy3-Aptamer. Besides, the in-tube reaction time of BPA was optimized (Fig. 3-D and Figs. S8–D). A micro-sample of BPA with a volume of 30 μL of was injected into the aptasensor at different flow rates to obtain different reaction times. The competitive elution of Cy3-aptamer was well carried out by BPA at the flow rate of 3 μL/min and the injection time was controlled in 10 min.

3.5. Sensitivity and specificity of SERS aptasensor

Under the optimal conditions, a series of BPA standard solutions were used to evaluate the analysis performance of the obtained SERS aptasensor. As shown in Fig. 4-A, the signal intensity gradually decreased with the increasing content of BPA in the range from 2.3 × 10^{-3} to 2.3 × 10^3 ng/L, based on the significant affinity specificity of aptamers toward the target BPA. The release of Cy3-Aptamer led to the drastic decrease of the SERS signal, and the excellent linear response between SERS signal change and BPA content was obtained with the coefficient of determination (R^2) as 0.9922 (in Fig. 4-B). The error bars in a good scale were calculated from the standard deviation of the average SERS intensity obtained by three measurements. The residual plot (in Fig. S9) showed that almost all the computed residuals were within the ±2 limits. The same could be observed in the case of response factors (in Fig. S10), and almost values were included between ±15% except for that of the high concentration level of 1.0 × 10^{-8} mol/L (2.28 × 10^3 ng/L). The measured data lie within reasonable limits, which indicates that the linearity can be assured over the calibration range [44]. According to references [45,46], the limit of detection (LOD) and limit of quantitation (LOQ) (Section S2.4and Table S3 in ESI) of this SERS aptasensor for BPA were calculated as 9.12 × 10^{-4} ng/L and 2.28 × 10^{-3} ng/L, respectively. The proposed SERS aptasensor could provide

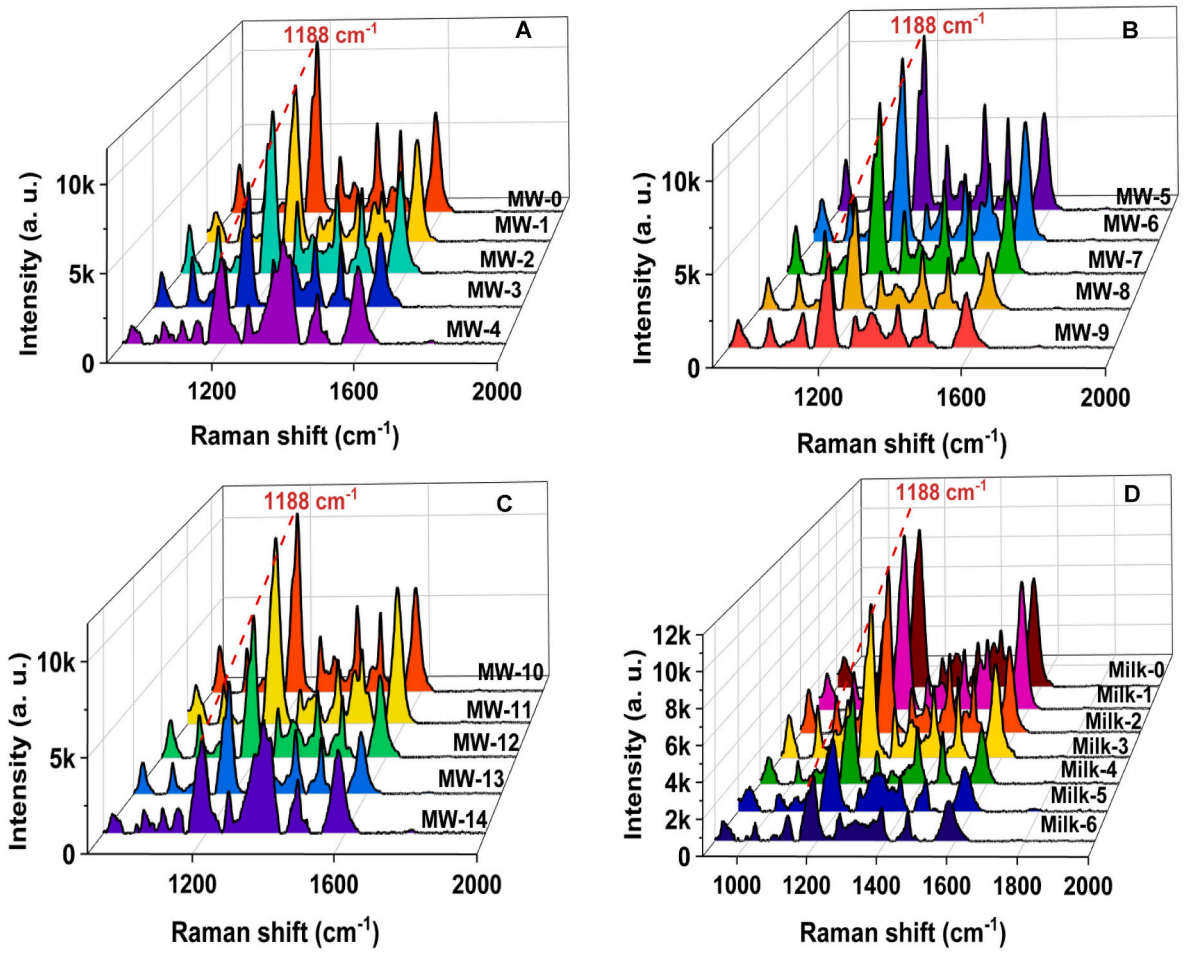


Fig. 6. Raman spectra of the 3D SERS aptasensor for BPA analysis in various samples
A, B and C: 15 simulated mineral water samples, D: 7 simulated milk samples.

Table 3
Determination of BPA in the heated mineral water and milk samples by using the monolithic SERS aptasensor and LC-MS/MS method.

Sample	Raman		LC-MS/MS		Sample	Raman		LC-MS/MS	
	Detected concentration (ng/L, n = 3)	RSD (%, n = 3)	Detected concentration (ng/L, n = 3)	RSD (%, n = 3)		Detected concentration (ng/L, n = 3)	RSD (%, n = 3)	Detected concentration (ng/L, n = 3)	RSD (%, n = 3)
MW-0	N.D.[a]	N.D.	N.D.[a]	N.D.	MW-11	N.D.	N.D.	N.D.	N.D.
MW-1	N.D.	N.D.	N.D.	N.D.	MW-12	8.16×10^{-2}	1.0	N.D.	N.D.
MW-2	N.D.	N.D.	N.D.	N.D.	MW-13	5.86	2.9	5.95	3.2
MW-3	3.88×10^{-1}	2.0	N.D.	N.D.	MW-14	8.16×10	1.4	8.09×10	0.4
MW-4	4.24×10^{-2}	4.4	4.18	7.6	Milk-0	N.D.	N.D.	N.D.	N.D.
MW-5	N.D.	N.D.	N.D.	N.D.	Milk-1	N.D.	N.D.	N.D.	N.D.
MW-6	N.D.	N.D.	N.D.	N.D.	Milk-2	N.D.	N.D.	N.D.	N.D.
MW-7	2.51×10^{-3}	2.0	N.D.	N.D.	Milk-3	7.82×10^{-3}	2.7	N.D.	N.D.
MW-8	3.12	5.3	3.19	2.5	Milk-4	1.33×10^{-1}	3.7	N.D.	N.D.
MW-9	5.40×10	4.3	5.47×10	7.2	Milk-5	7.27×10^{2}	6.9	7.03×10^{2}	7.2
MW-10	N.D.	N.D.	N.D.	N.D.	Milk-6	1.49×10^{3}	1.7	1.46×10^{3}	4.3

[a] : N.D.: Not detected, or under the LOD.

a platform for rapid and ultrasensitive detection of BPA.

The ability of specific recognition of the aptasensor towards the target was crucial for the accuracy of the detection. To evaluate the specificity of the monolithic SERS aptasensor, the Raman spectra were recorded for several potential analogues including BP, BPB, and BPC. The mixtures of analogues with or without BPA were also investigated. Fig. 4-B clearly showed that there was no obvious Raman intensity change at 1188 cm^{-1} compared to the blank for these interfering substances and their mixture without BPA. For the analyte of BPA, there was a significant decrease in the Raman intensity at 1188 cm^{-1} compared to the blank, as highlighted that the proposed aptasensor displayed a great specificity towards BPA. Moreover, as shown in Fig. 4-B, the Raman

Table 4
Comparison of the BPA analysis results proceeded by the reported SERS aptasensors with this work.

SERS sensors/probes	Substrate category	Sample	Sample volume (μL)	Recognition time (min)	LOD (ng/L)	RSD (%)	Recovery (%)	Ref.
AuNPs - AuNRs based SERS aptasensor	solution-based substrate	Tap-water	100	720	3.88	N.D.	91–95.3	[40]
GOx-AuNSs based SERS aptasensor	solution-based substrate	Tap-water	100	120	5.01×10^{-5}	3.3–5.7	93.8–103.1	[48]
Single-atom catalyst amplification AuNPs SERS/RRS as aptasensor	solution-based substrate	plastic wrap, disposable plastic cups, black plastic bags, and plastic gloves	200	50	4.56	5.1–7.9	90–103	[49]
Aptamer-embedded Au/Ag core-shell nanoprobes (NPs)	glass tube-based substrate	N.D.	N.D.	40	2.28×10^{-3}	N.D.	N.D.	[35]
Au@cDNA@Ag@Aptamer NPs monolithic aptasensor	capillary monolith-based substrate	River water, Mineral water bottles, and Milk	30	10	7.53×10^{-4}	4.76–5.18	94.1–104.5	This work

N.D.: could not be detected, or data could not be provided.

signal of the mixture composed of analogues and BPA was nearly identical to that of BPA, which indicated that the quantitative detection of BPA in complex solutions with a high accuracy could be achieved using this monolithic SERS aptasensor.

3.6. Stability and reproducibility

The stability and reproducibility of the Raman intensity are important for accurate detection in applications. In Fig. 4-D, the SERS spectra were collected from 30 random spots on a monolithic SERS aptasensor, and the corresponding distribution diagram for the SERS intensity at 1188 cm^{-1} was displayed in Fig. S11. A relative standard deviation (RSD) of the same segment (spot-to-spot, n = 30) was achieved as 4.76% and indicated excellent reproducibility. The stability was also studied by testing three segments in a monolith (unit to unit, n = 3), the SERS monoliths from the same batch (column-to-column) and different batches (batch-to-batch). Fig. S12 and Table S4 showed the RSD of column-to-column (n = 3), and batch-to-batch (n = 3) of the SERS signal at 1188 cm^{-1} was 5.05% and 5.18%, respectively. All above indicated that this monolithic SERS aptasensor had a great reproducibility and robust stability of SERS intensity for the quantitative specific microanalysis of BPA..

3.7. Sample analysis

To examine the performance of the SERS aptasensor for practical application, the analysis of various samples with the developed SERS aptasensor is considered. As shown in Fig. 5Ã C, the monolithic SERS aptasensor exhibited a highly sensitive detection of BPA in the fortified river water samples. No significant interferences were observed from the SERS spectra of BPA in the fortified river water. The average recovery yields of BPA in the fortified river water and milk samples were calculated in the ranges of 94.1 ± 5.8%–104.5 ± 7.3% (n = 3) (in Table 1) and 91.0 ± 7.9%–109 ± 5.5% (n = 3) (in Table 2), respectively, as indicated that the 3D SERS aptasensor was capable to detect trace BPA in river water and milk samples.

Additionally, a series of simulated products including bottled mineral water and box milk packed with plastic-based polymer material were adopted and the content of BPA was detected, respectively. These mineral water and milk samples were prepared under different simulated heating statuses of 70 °C–40 °C for 1∼5 h and 95 °C–50 °C for 5min, respectively. As shown in Fig. 6 A-D and Fig. S13, the SERS signal intensity was gradually decreased with the heating temperature and heating time increasing respectively, which indicated that high temperature and heating time could promote the release of BPA from the plastic-based polymer bottles, as well as the milk package box. No significant interferences were found between the SERS spectra of BPA in these water samples and milk samples treated under the simulated heating process. In Table 3, the contents of BPA released from the plastic package of water and milk samples were found in 2.51×10^{-3} ng/L ∼1.49×10^{3} ng/L by using the monolithic SERS sensing platform. The results obtained were confirmed by the LC-MS method. As shown in Table 3, there was no significant difference in the detection results between the two methods. Trace BPA in heated water and milk samples could be well identified with the error ban in a good range, which further verified that this method could identify trace BPA pollutants with super sensitivity, high specificity, and good accuracy.

Meanwhile, the analytical methods were evaluated based on the RGB evaluation model (Section S2.8, in ESI). The scores obtained in the REDNESS, GREENNESS, and BLUENESS sections were 70.7, 91.5, and 80.8, respectively (in Table S5). The final brilliance of 80.5 was achieved and the final colour was white. It lighted that this method might conform to the three concepts of analytical performance, safety and eco-friendliness, and productivity/practical effectiveness.

Besides, the enhancement factor (EF) was calculated and shown in Section S2.6 in ESI. The EF was calculated as 2.95×10^{8}. The comparison of the proposed method with the previous SERS aptasensors for the microanalysis of BPA was also proceeded and shown in Table 4. The proposed monolithic SERS aptasensor has the obvious advantages in a faster recognition time (only 10 min) and better sensitivity for BPA detection in comparison of most the reported traditional solution-based or planar substrate-based aptasensors, owing to the substantially higher recognition and capture efficiency of the 3D-monolith and the unique structure of the capillary monolith [40,47–49]. The recognition of this SERS platforms suffered from a tedious recognition period from 40 min to 120 min even 720 min, was avoided. It required a short test time and greatly promoted the analysis efficiency. This monolithic SERS aptasensor possessed a high-performance property and could be particularly potential for the rapid quantitative detection of trace BPA in microanalysis.

4. Conclusions

In this work, a novel 3D monolithic structure-substrate SERS platform functionalized with Au@cDNA@Ag@Cy3-Apt NPs was exploited and used for the high-performance test of trace BPA. The monolithic porous structure decorated with Au@cDNA@Ag@Cy3-Apt NPs was finely regulated and exhibited a highly specific affinity recognition toward BPA (in 10 min) with a significant change of SERS signal. Using the facile Ag-shell regulation, Au@Ag NPs were finely tuned to maintain excellent SERS hotspot sensing performance of Raman tag Cy3 to achieve ultra-high SERS sensitivity. The advantages of capillary 3D-substrate SERS such as signal amplification, high capture efficiency, and aptamer-affinity recognition, were integrated, which resulted in ultra-high sensitivity, high specificity, and excellent reproducibility. Furthermore, a rapid analysis process was accomplished in 10 min,

which was better than most traditional planar or solution-based SERS sensors. Under the optimal conditions, the enhancement factor (EF) was calculated as 2.95×10^8, and ultra-high sensitivity for BPA analysis was achieved with LOD and LOQ of 9.12×10^{-4} ng L^{-1} and 2.28×10^{-3} ng L^{-1}, respectively. Applied to natural samples, the robust applications were validated. There was no significant difference between the proposed SERS and LC-MS/MS methods. Although the 3D structure of the monolith requires fine control, this proposed SERs method could identify trace BPA residue with high sensitivity and good accuracy. It might open a new approach towards a capillary aptamer-affinity monolith acting as a SERS sensing platform for the ultrasensitive and highly-specific determination of BPA.

Author contributions

Zhixin Li and Qian Xie: data curation, formal analysis, and writing - original draft. Jinxin Chi: data curation, and formal analysis. Hui Chen: data curation. Zhuling Chen: data curation. Xucong Lin: conceptualization, validation, funding acquisition, supervisor, and writing - review and editing. Guihua Huang: supervisor, and writing - review and editing.

Declaration of competing interest

The authors declare that they have no known competing financial interests or personal relationships that could have appeared to influence the work reported in this paper.

Data availability

Data will be made available on request.

Acknowledgment

The work was funded by Scientific Research and Develop Project of Fujian Province 2020Y4004, 2020R1013001, 2021Y0043), Fujian Provincial Ocean Development Fund (FJHJF-L-2022-13).

Appendix A. Supplementary data

Supplementary data to this article can be found online at https://doi.org/10.1016/j.talanta.2023.125081.

References

[1] X.L. Zhang, D. Wu, X.X. Zhou, Y.X. Yu, J.C. Liu, N. Hu, H.L. Wang, G.L. Li, Y.N. Wu, Recent progress in the construction of nanozyme-based biosensors and their applications to food safety assay, Trac-Trend. Anal. Chem. 121 (2019), 115668, https://doi.org/10.1016/j.trac.2019.115668.

[2] R.V. Nair, P.R. Chandran, P. Mohamed, S. Pilla, Sulphur-doped graphene quantum dot based fluorescent turn-on aptasensor for selective and ultrasensitive detection of omethoate, Anal. Chem. Acta. 1181 (2021), 338893, https://doi.org/10.1016/j.aca.2021.338893.

[3] G.W. Xing, W.F. Zhang, N. Li, Q.S. Pu, J.M. Lin, Recent progress on microfluidic biosensors for rapid detection of pathogenic bacteria, Chin. Chem. Lett. 33 (2022) 1743–1751, https://doi.org/10.1016/j.cclet.2021.08.073.

[4] X.M. Li, M.M. Ni, Z.R. Yang, X.X. Chen, L.S. Zhang, J.Y. Chen, Bioinformatics analysis and quantitative weight of evidence assessment to map the potential mode of actions of bisphenol A, Environ. Pollut. 273 (2021), 116469, https://doi.org/10.1016/j.envpol.2021.116469.

[5] Y.Y. Zhang, W.W. Zhang, L.M. Zhang, G.S. Song, N.W. Wang, W.Z. Xu, W. H. Huang, A molecularly imprinted electrochemical BPA sensor based on multi-walled carbon nanotubes modified by CdTe quantum dots for the detection of bisphenol A, Micochem. J. 170 (2021), 106737, https://doi.org/10.1016/j.microc.2021.106737.

[6] S. Sahin, Z. Ustundag, M.O. Caglayan, Spectroscopic ellipsometry-based aptasensor platform for bisphenol a detection, Talanta 253 (2023), 123885, https://doi.org/10.1016/j.talanta.2022.123885.

[7] C.Y. Wang, Y. Zeng, A.G. Shen, J.M. Hu, A highly sensitive SERS probe for bisphenol A detection based on functionalized Au@Ag nanoparticles, Anal. Methods 10 (2018) 5622–5628, https://doi.org/10.1039/c8ay01966e.

[8] K. Czarny-Krzyminska, B. Krawczyk, D. Szczukocki, Bisphenol A and its substitutes in the aquatic environment: occurrence and toxicity assessment, Chemosphere 315 (2023), 137763, https://doi.org/10.1016/j.chemosphere.2023.137763.

[9] Q.Y. Wang, L.F. Chen, X.Y. Cui, J. Zhang, Y.H. Wang, X.P. Yang, Determination of trace bisphenols in milk based on Fe3O4@NH2-MIL-88(Fe)@TpPa magnetic solid-phase extraction coupled with HPLC, Talanta 256 (2023), 124268, https://doi.org/10.1016/j.talanta.2023.124268.

[10] M. Rezaee, Y. Yamini, S. Shariati, A. Esrafili, M. Shamsipur, Dispersive liquid-liquid microextraction combined with high-performance liquid chromatography-UV detection as a very simple, rapid and sensitive method for the determination of bisphenol A in water samples, J. Chromatogr. A 1216 (2009) 1511–1514, https://doi.org/10.1016/j.chroma.2008.12.091.

[11] X.L. Zhou, J.P. Kramer, A.M. Calafat, X.Y. Ye, Automated on-line column-switching high performance liquid chromatography isotope dilution tandem mass spectrometry method for the quantification of bisphenol A, bisphenol F, bisphenol S, and 11 other phenols in urine, J. Chromatogr. B 944 (2014) 152–156, https://doi.org/10.1016/j.jchromb.2013.11.009.

[12] Y. Deceuninck, E. Bichon, S. Durand, N. Bemrah, Z. Zendong, M.L. Morvan, P. Marchand, G. Dervilly-Pinel, J.P. Antignac, J.C. Leblanc, B. Le Bizec, Development and validation of a specific and sensitive gas chromatography tandem mass spectrometry method for the determination of bisphenol A residues in a large set of food items, J. Chromatogr. A 1362 (2014) 241–249, https://doi.org/10.1016/j.chroma.2014.07.105.

[13] M.M. Arce, M.C. Ortiz, S. Sanllorente, HPLC-DAD and PARAFAC for the determination of bisphenol-A and another four bisphenols migrating from BPA-free polycarbonate glasses, Microchem. J. 168 (2021), 106413, https://doi.org/10.1016/j.microc.2021.106413.

[14] T. Tuzimski, S. Szubartowski, R. Gadzala-Kopciuch, A. Miturski, M. Wojtowicz-Marzec, W. Kwasniewski, B. Buszewski, Comparison of DAD and FLD detection for identification of selected bisphenols in human breast milk samples and their quantitative analysis by LC-MS/MS, J. AOAC Int. 103 (2020) 1029–1042, https://doi.org/10.1093/jaoacint/qsaa027.

[15] L.K. Lin, L.A. Stanciu, Bisphenol A detection using gold nanostars in a SERS improved lateral flow immunochromatographic assay, Sensor Actuat B-Chem. 276 (2018) 226–229, https://doi.org/10.3390/nano12081374.

[16] Y.Q. Xie, L. Ma, S.M. Ling, H.X. Ouyang, A.H. Liang, Z.L. Jiang, Aptamer-adjusted carbon dot catalysis-silver nanosol SERS spectrometry for bisphenol A detection, Nanomaterials 12 (2022) 1374, https://doi.org/10.3390/nano12081374.

[17] L.B. Yang, Y.L. Chen, Y. Shen, M. Yang, X.L. Li, X.X. Han, X. Jiang, B. Zhao, SERS strategy based on the modified Au nanoparticles for highly sensitive detection of bisphenol A residues in milk, Talanta 179 (2018) 37–42, https://doi.org/10.1016/j.talanta.2017.10.055.

[18] W.M. Yin, L. Wu, F. Ding, Q. Li, P. Wang, J.J. Li, Z.C. Lu, H.Y. Han, Surface-imprinted SiO2@Ag nanoparticles for the selective detection of BPA using surface enhanced Raman scattering, Sensor Actuat B-Chem. 258 (2018) 566–573, https://doi.org/10.1016/j.snb.2017.11.141.

[19] C.Y. Wang, Y. Zeng, A.G. Shen, J.M. Hu, A highly sensitive SERS probe for bisphenol A detection based on functionalized Au@Ag nanoparticles, Anal. Methods 10 (2018) 5622–5628, https://doi.org/10.1039/c8ay01966e.

[20] S.Y. Huang, W.N. Gao, C.M. Chou, V.K.S. Hsiao, Porous silicon decorated with Au/TiO2 nanocomposites for efficient photoinduced enhanced Raman spectroscopy, RSC Adv. 13 (2023) 15634–15639, https://doi.org/10.1039/d3ra02598e.

[21] L. Jiang, M.M. Hassan, S. Ali, H.H. Li, R. Sheng, Q.S. Chen, Evolving trends in SERS-based techniques for food quality and safety: a review, Trends Food Tech 112 (2021) 225–240, https://doi.org/10.1016/j.tifs.2021.04.006.

[22] A. Garg, W. Nam, W. Zhou, Reusable surface-enhanced Raman spectroscopy membranes and textiles via template-assisted self-assembly and micro/nanoimprinting, ACS Appl. Mater. Interfaces 12 (2020) 56290–56299, https://doi.org/10.1021/acsami.0c16351.

[23] Q.Q. Li, Y.P. Du, H.R. Tang, X. Wang, G.P. Chen, J. Iqbal, W.M. Wang, W.B. Zhang, Ultra sensitive surface-enhanced Raman scattering detection based on monolithic column as a new type substrate, J. Raman Spectrosc. 43 (2012) 1392–1396, https://doi.org/10.1002/jrs.4095.

[24] J.W. Jeong, M.M.P. Arnob, K.M. Baek, S.Y. Lee, W.C. Shih, Y.S. Jung, 3D cross-point plasmonic nanoarchitectures containing dense and regular hot spots for surface-enhanced Raman spectroscopy analysis, Adv. Mater. 28 (2016) 8695–8704, https://doi.org/10.1002/adma.201602603.

[25] Y. Chang, P. Liang, Q.M. Dong, D. Zhang, J. Xia, Y.F. Zhou, Z. Yu, J. Huang, D.J. Ni, S.Z. Jin, Highly sensitivity and homogeneous SERS platforms based on 3D-GNF/AgNPs hybrid structures, Mater. Res. Express.https://doi.org/10.1088/2053-1591/ab057f.

[26] G. Biasotto, A. Chiad, C. Novara, M. Fontana, M. Armandi, M.A. Zaghete, F. Giorgis, P. Rivolo, Graphenic aerogels decorated with ag nanoparticles as 3d sers substrates for biosensing, Part. Part. Syst. Char. 37 (2020), 2000095, https://doi.org/10.1002/ppsc.202000095.

[27] J.W.M. Osterrieth, D. Wright, H. Noh, C.W. Kung, D. Vulpe, A. Li, J.E. Park, R. P. Van Duyne, P.Z. Moghadam, J.J. Baumberg, O.K. Farha, D. Fairen-Jimenez, Core-shell gold nanorod @ zirconium-based metal-organic framework composites as in situ size-selective Raman probes, J. Am. Chem. Soc. 141 (2019) 3893–3900, https://doi.org/10.1021/jacs.8b11300.

[28] J.X. Chi, C.C. Xia, Z.Y. Guo, G.H. Huang, X.C. Lin, Gold nanoparticle-decorated porous silica for surface-enhanced Raman scattering-based detection of trace molecules in liquid phase, ACS Appl. Nano Mater. 5 (2022) 527–536, https://doi.org/10.1021/acsanm.1c03324.

[29] Q. Jiang, T. Zeng, S. Yang, Q. Chen, L. Chen, Y. Ye, J. Zhou, S.P. Xu, On-column enrichment and surface-enhanced Raman scattering detection in nanoparticles

functionalized porous capillary monolith, Spectrochim. Acta A. 141 (2015) 244–251, https://doi.org/10.1016/j.saa.2015.01.044.
[30] Y. Li, M.X. Guo, L. He, C.Z. Huang, Y.F. Li, Green one-pot synthesis of silver nanoparticles/metal-organic gels hybrid and its promising SERS application, ACS Sustainable Chem. Eng. 7 (2019) 5292–5299, https://doi.org/10.1021/acssuschemeng.8b06305.
[31] L. Zhou, Y.Y. Peng, N. Zhang, R. Du, R. Hubner, X.L. Wen, D.H. Li, Y. Hu, A. Eychmuller, Size-tunable gold aerogels: a durable and misfocus-tolerant 3D substrate for multiplex SERS detection, Adv. Opt. Mater. 9 (2021), 2100352, https://doi.org/10.1002/adom.202100352.
[32] Y.S. Wang, L. Polavarapu, L.M. Liz-Marzán, Reduced graphene oxide-supported gold nanostars for improved SERS sensing and drug delivery, ACS Appl. Mater. Interfaces 6 (2014) 21798–21805, https://doi.org/10.1021/am501382y.
[33] H.K. Lee, Y.H. Lee, C.S.L. Koh, G.C. Phan-Quang, X.M. Han, C.L. Lay, H.Y.F. Sim, Y. C. Kao, Q. An, X.Y. Ling, Designing surface-enhanced Raman scattering (SERS) platforms beyond hotspot engineering: emerging opportunities in analyte manipulations and hybrid materials, Chem. Soc. Rev. 48 (2019) 731–756, https://doi.org/10.1039/c7cs00786h.
[34] H. J, Gruber, C.D. Hahn, G. Kada, C.K. Riener, G.S. Harms, W. Ahrer, T.G. Dax, H. G. Knaus, Anomalous fluorescence enhancement of Cy3 and Cy3.5 versus anomalous fluorescence loss of Cy5 and Cy7 upon covalent linking to IgG and noncovalent binding to avidin, Bioconjugate Chem. 11 (2000) 696–704, https://doi.org/10.1021/bc000015m.
[35] E. Chung, J. Jeon, J.M. Yu, C. Lee, J. Choo, Surface-enhanced Raman scattering aptasensor for ultrasensitive trace analysis of bisphenol A, Biosens. Bioelectron. 64 (2015) 560–565, https://doi.org/10.1016/j.bios.2014.09.087.
[36] H. Pu, X. Xie, D.W. Sun, Q. Wei, Y. Jiang, Double strand DNA functionalized Au@Ag NPs for ultrasensitive detection of 17β-estradiol using surface-enhanced Raman spectroscopy, Talanta 195 (2019) 419–425, https://doi.org/10.1016/j.talanta.2018.10.021.
[37] M. Kasztelan, A. Sloniewska, M. Gorzkowski, A. Lewera, B. Palys, S. Zoladek, Ammonia modified graphene oxide - gold nanoparticles composite as a substrate for surface enhanced Raman spectroscopy, Appl. Surf. Sci. 554 (2021), 149060, https://doi.org/10.1016/j.apsusc.2021.149060.
[38] Y.F. Ye, X.Y. Qi, H. Wang, B.B. Zhao, L.X. Xu, Y.T. Zhang, X.L. Wang, N.D. Zhou, A surface-enhanced Raman scattering aptasensor for Escherichia coli detection based on high-performance 3D substrate and hot spot effect, Anal. Chim. Acta 1221 (2022), 340141, https://doi.org/10.1016/j.aca.2022.340141.
[39] F. Lu, J. Lin, C. Lin, G. Qi, X. Lin, Z. Xie, Heteroporous 3D covalent organic framework-based magnetic nanospheres for sensitive detection of bisphenol A, Talanta 231 (2021), 122343, https://doi.org/10.1016/j.talanta.2021.122343.
[40] J.J. Feng, L.G. Xu, G. Cui, X.L. Wu, W. Ma, H. Kuang, C.L. Xu, Building SERS-active heteroassemblies for ultrasensitive Bisphenol A detection, Biosens. Bioelectron. 81 (2016) 138–142, https://doi.org/10.1016/j.bios.2016.02.055.
[41] Y.L. Wang, K. Lee, J. Irudayaraj, SERS aptasensor from nanorod-nanoparticle junction for protein detection, Chem. Commun. 46 (2010) 613–615, https://doi.org/10.1039/b919607b.
[42] Y.L. Wang, K. Lee, J. Irudayaraj, SERS aptasensor from nanorod-nanoparticle junction for protein detection, Chem. Commun. 46 (2010) 613–615. https://10.1039/b919607b.
[43] Y. Wu, T. Jiang, Z. Wu, R. Yu, Novel ratiometric surface-enhanced Raman spectroscopy aptasensor for sensitive and reproducible sensing of Hg2+, Biosens. Bioelectron. 99 (2018) 646–652, https://doi.org/10.1016/j.bios.2017.08.041.
[44] J.M. Jurado, A. Alcazar, R. Muniz-Valencia, S.G. Ceballos-Magana, F. Raposo, Some practical considerations for linearity assessment of calibration curves as function of concentration levels according to the fitness-for-purpose approach, Talanta 172 (2017) 221–229, https://doi.org/10.1016/j.talanta.2017.05.049.
[45] IUPAC, Compendium of chemical terminology, in: The "Gold Book", Blackwell Scientifific Publications, Oxford, UK, 1997, 0-9678550-9-8.
[46] Á. Lavín, J. Vicente, M. Holgado, M. Laguna, R. Casquel, B. Santamaría, On the Determination of Uncertainty and Limit of Detection in Label-free, Biosensors, 2018, pp. 1–18, https://doi.org/10.3390/s18072038.
[47] H.Y. Shi, N. Chen, Y.Y. Su, H.Y. Wang, Y. He, Reusable silicon-based surface-enhanced Raman scattering ratiometric aptasensor with high sensitivity, specificity and reproducibility, Anal. Chem. 89 (2017) 10279–10285, https://doi.org/10.1021/acs.analchem.7b01881.
[48] Z. Xu, R. Wang, B. Mei, L. Ding, L.B. Wang, M.L. Chen, Y.H. Cheng, A surface-enhanced Raman scattering active core/shell structure based on enzyme-guided crystal growth for bisphenol A detection, Anal. Methods 10 (2018) 3878–3883, https://doi.org/10.1039/C7AY02776A.
[49] D. Li, C.N. Li, H.L. Wang, J. Li, Y.X. Zhao, X. Jiang, G.Q. Wen, A.H. Liang, Z. L. Jiang, Single-atom Fe catalytic amplification-gold nanosol SERS/RRS aptamer as platform for the quantification of trace pollutants, Microchim. Acta 188 (2021) 175, https://doi.org/10.1007/s00604-021-04828-8.